

Multi-lumen capillary based trypsin micro-reactor for the rapid digestion of proteins

Electronic supplementary information.

S.A. Currivan^a, W.Q. Chen^b, R. Wilson^c, E. Sanz Rodriguez^d, N. Upadhyay^a, D. Connolly^e, P.N. Nesterenko^{a,d}, and B. Paull^{a,d*}

- a.* Australian Centre for Research on Separation Science, School of Natural Sciences, University of Tasmania, Tasmania, Australia.
b. College of Biological and Environmental Engineering, Zhejiang Shuren University, Hangzhou 310015, China.
c. Central Science Laboratory, University of Tasmania, Sandy Bay, Hobart, Australia.
d. ARC Industrial Training Centre for Portable Analytical Separation Technologies (ASTech), School of Natural Sciences, University of Tasmania, Sandy Bay, Hobart, Tasmania, Australia.
e. APC, Cherrywood Business Park, Loughlinstown Co. Dublin, Ireland, D18 DH50

Comparison of MLC to fused silica capillaries:

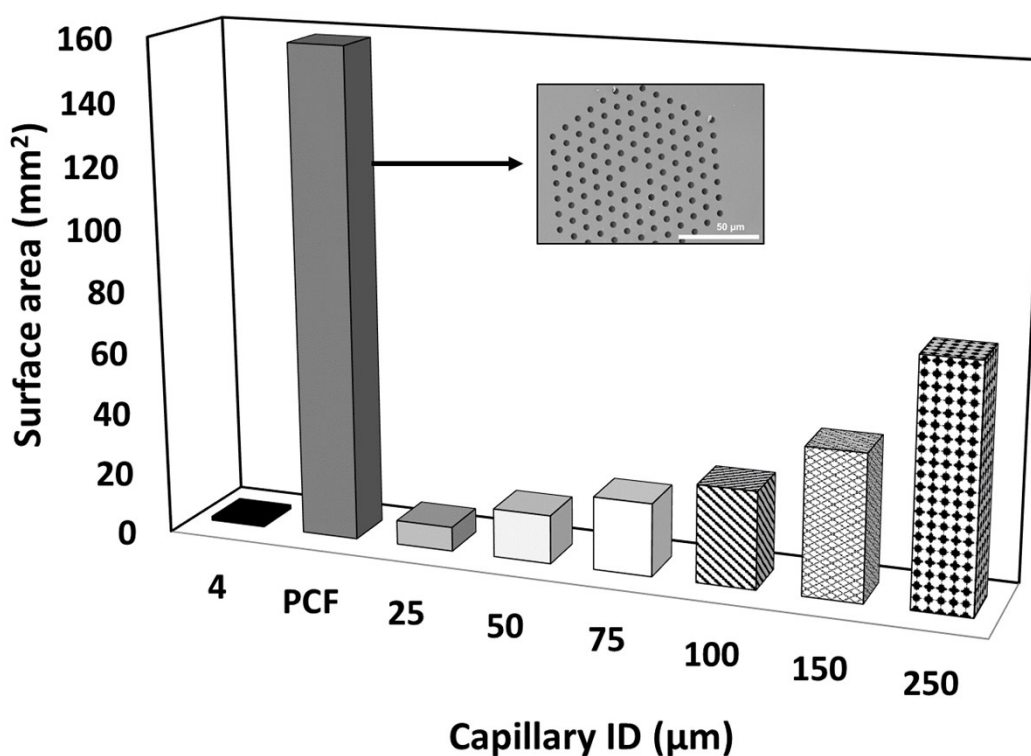


Figure S1: comparison of surface area between the MLC (PCF) and FSCs of increasing inner diameters, from 25 μm ID to 250 μm ID, for a hypothetical capillary length of 100 mm. Insert; SEM micrograph of MLC cross sectional area, showing the 126 x 4 μm I.D. channels.

SEM characterisation of AuNP coated MLC:

SEM microscopy was used to characterise the coverage of gold nanoparticles (AuNPs) in each channel, axially across the MLC. In order to achieve this, a number of AuNP modified MLCs were cut into sections and analysed. MLC channels with no AuNP modification are shown to possess smooth channel walls, and no edge effects were observed (i.e white line around the channel inner wall). The presence of AuNPs on the MLCs was indicated by a localised increase in emitted electrons due to changes in topography (edge effects) and an increase in conductivity due to the presence of AuNPs (brighter signal) around the inner surface of the channels. Upon closer inspection, the surface was also roughened, due to the presence of the AuNPs. When the capillary was rotated, the AuNPs appear as white spheres upon the surface similar to that previously reported upon aminated polymer surfaces¹, which at the angle of observation look to be a roughened surface along the inner wall of the MLC channel. Individual channels were mapped and the presence of gold was noted. The layer of 20nm particles is visible along the inner wall of the MLC channel. From a selection of the SEMs in Figure S2, the distribution of AuNPs was homogenous across the sections of MLC tested. If the angle of observation is changed, the inner wall of the capillary can be profiled, as shown in Figure 1.

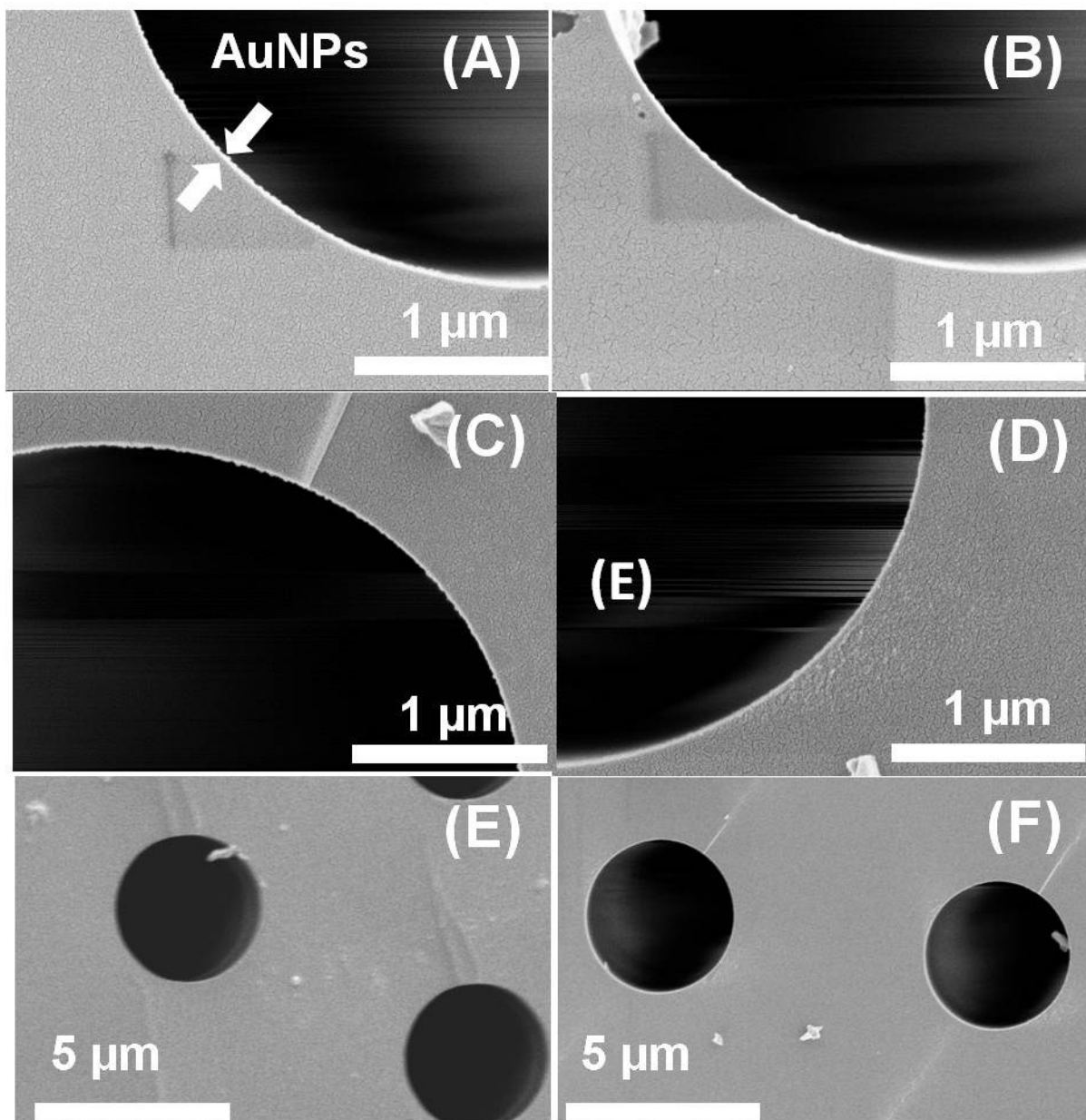


Figure S2: SEM characterisation of AuNP coating upon the inner walls of APTES modified MLC channels. AuNPs on the inner surface are highlighted in (A), and can be seen as a bright, rough lining on the MLC channel wall (B-D). SEM micrographs recorded at 45 k magnification and an accelerating voltage of 1.5 kV. Scale bars of 1 μm re shown in each micrograph. Samples were sputter coated with platinum prior to analysis. For comparison purposes, a blank MLC is shown (E), next to an AuNP MLC at 3 k magnification (F). The edge effect (white ring along the inner wall) due to the presence of the AuNP is notable absent in (E) while it is present in (F).

Table S1: compilation of conditions used in previous reports using IMERs of different media, and the effects of flow rate.

Monolith					
<i>IMER dimensions</i>	<i>Flow rate (μL/min)</i>	<i>Substrate</i>	<i>Temp.</i>	<i>Effect of flow rate on digestion</i>	<i>Reference</i>
0.1 mm x 100 mm ^a .	0.4-0.5	Melittin, cytochrome c, RNase A, myoglobin, casein, a-acid glycoprotein, bovine serum albumin (BSA), holo-transferrin	37 °C	N/A	2
0.02 mm x 0.05 mm x 20 mm ^b . 0.1 mm x 20 mm ^a .	0.5	N-α-benzoyl-L-arginine (BAEE), myoglobin, casein.	N/A	No	3
0.075 mm x 25 mm ^a .	0.05-0.30	Cytochrome c	N/A	Yes	4
4.6 mm x 50 mm ^c .	100-1000	Polynucleotides, poly(c) and RNA	22 and 35 °C	No	5
4.6 mm x 50 mm ^c .	100-500	BAEE, myoglobin	21, 30, and 37 °C	Yes	6
0.1 mm x 300 mm ^a .	0.10-0.30	BAEE, BSA, lysozyme, cytochrome c, human peroxisome proliferator-activated receptor α, β-lactoglobulin, and myoglobin	37 °C	Yes/no *	7
CIMac™ disk 5.2 mm x 5 mm	300-1500	Cytochrome C, ovalbumin, BSA, Human serum albumin	RT**	Yes	8
Silica hybrid monolith, 0.1 mm x 10 mm	0.3-5.0	Myoglobin	RT	Yes	9
Membrane					
40 mm long	0.1-0.3	Cytochrome c	RT	Yes	10
2 x 5 mm placed over an open 0.05 mm I.D. capillary.	0.10-0.01	Cytochrome c, ovalbumin	37 °C	No	11
Particulate					
1 mm x 0.25 mm x 20 mm ^b , 500 nm particles.	0.167-0.667	Cytochrome C	25 °C	Yes	12
0.53 mm x 300 mm ^a . Beads; 150-180 μm.	0.15-0.25	Insulin chain B (oxidised), β casein	37 °C	Yes	13
0.8 mm x 0.15 mm x 15 mm long ^b , 40-60 μm beads.	0.5-60	Melittin, cytochrome C, bovine serum albumin	N/A	Yes	14
Ependorph reactor, 1.5 μm beads	N/A	<i>E. Coli</i> , MCF7 Cell lysate	37 °C	N/A	15
9 channels, 1mm x 10 mm x 0.035 mm. 5 μm beads with 100 Å pores.	1	BSA, myoglobin, lysozyme, hemoglobin	RT	N/A	16
0.25 mm I.D., 10 μm beads, 1 nm pores.	1	<i>E. Coli</i> , BSA	RT	N/A	17
Open channel					
0.05 mm x 500 mm ^a .	0.04	β casein	N/A	Yes	18
0.075 μm x 220 mm, 0.05 mm x 510 mm, or 0.05 mm x 1400 mm ^a .	1-5	Cytochrome C, myoglobin	37 °C	Yes	19

^a capillary format, ^b microfluidic chip format, ^c stainless steel tube housing. * Also limited by the size of the protein used, the larger the protein, the greater the effect of flow rate upon digestion efficiency. ** RT room temperature.

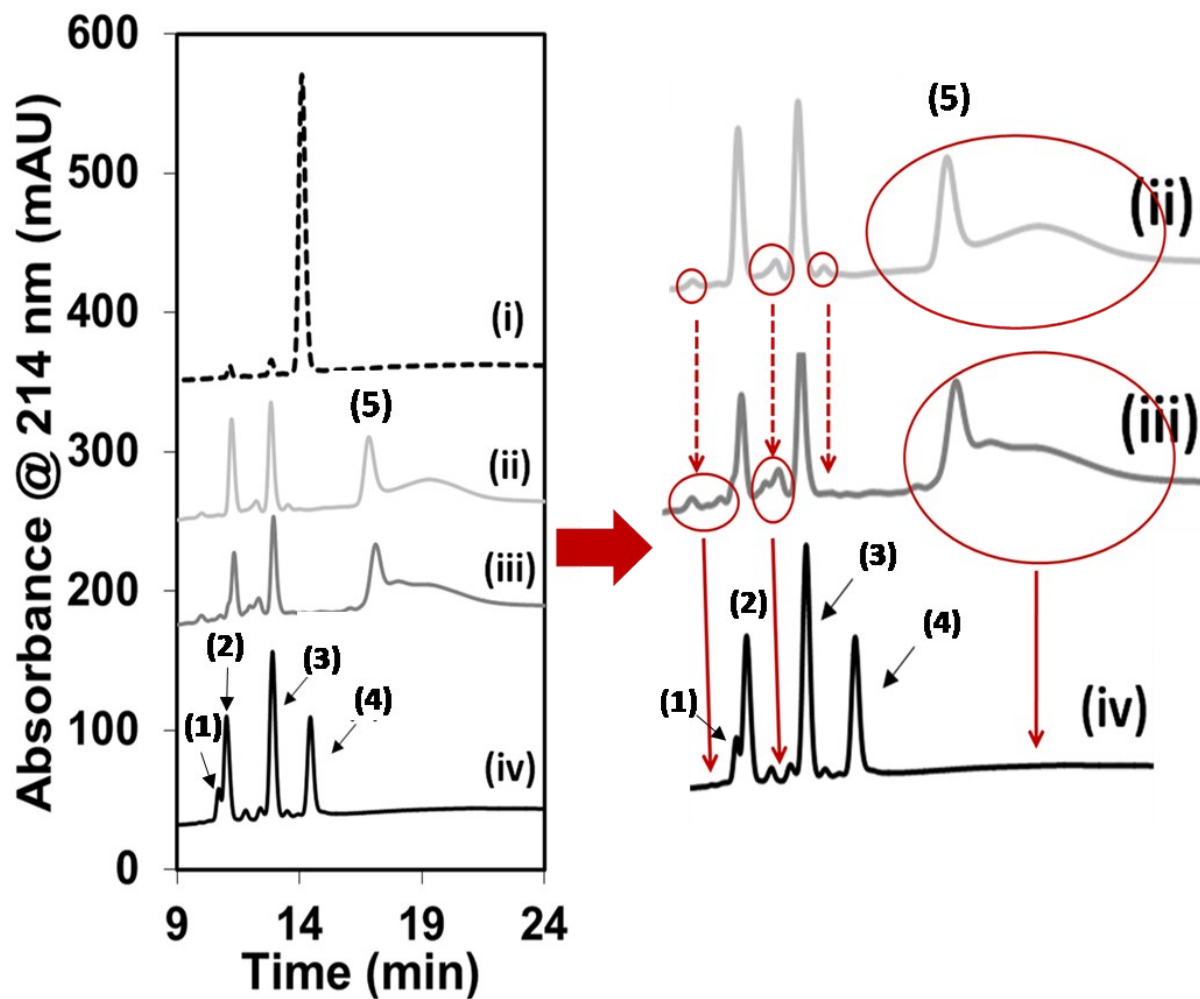


Figure S3: Chromatogram of insulin oxidised chain B (i), in vitro digest after 5 min incubation (ii), after 18 h incubation (iii), and a digest obtained using the MLC-IMER at a flow rate of 0.1 $\mu\text{L}/\text{min}$ (iv). Traces (ii)-(iv) are enlarged to demonstrate the presence of additional peaks due to trypsin, with broad peaks seen between 15 and 20 min, due to the presence of the enzyme.

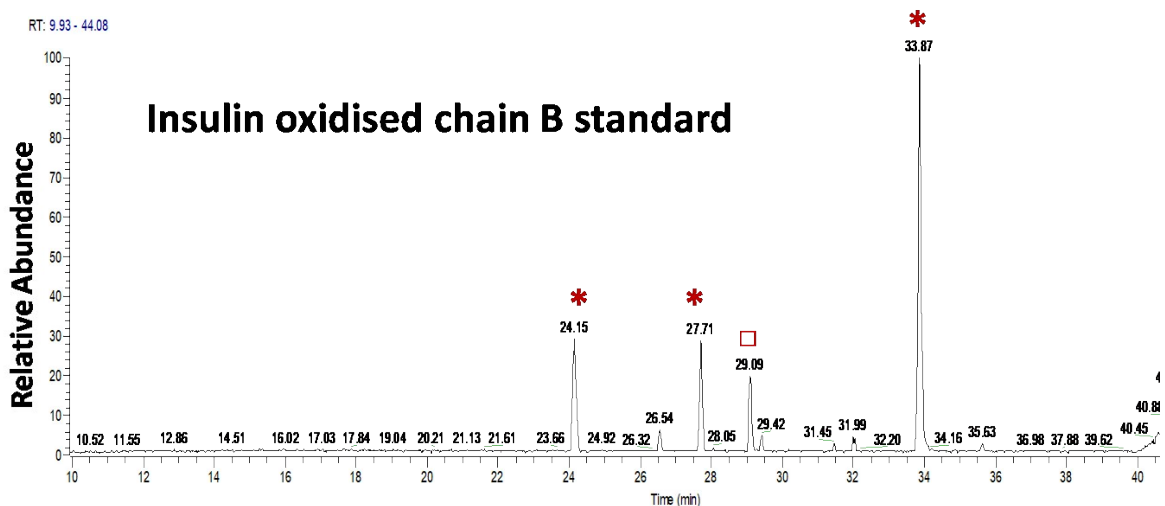


Figure S4: Base peak chromatograms of the insulin standard. Peaks due to the protein are denoted with *. The unidentified peak with an m/z ratio of 939.4490 is shown with \square . The protein was loaded onto a 20 mm x 75 μm sample trapping column (Acclaim PepMap 3 μm C18) then separated over a 45 minute gradient from 2% acetonitrile to 50% acetonitrile on a 250 mm x 75 μm RSLC analytical column (Acclaim PepMap 2 μm C18). The LTQ-Orbitrap was controlled using Xcalibur 2.1 software and base peak chromatograms showing FTMS signal intensity were annotated using Qual Browser software.

The peaks of the insulin chain B standard were analysed. The resulting peaks at 24.15 and 27.71 demonstrate some inherent degradation of the protein. This could also be seen in the nanoLC traces shown in Figure 3 of the main text. The degradation of the protein may have contributed to the issues observed with the lysing of the alanine site, responsible for the fragment of 930.4719 m/z .

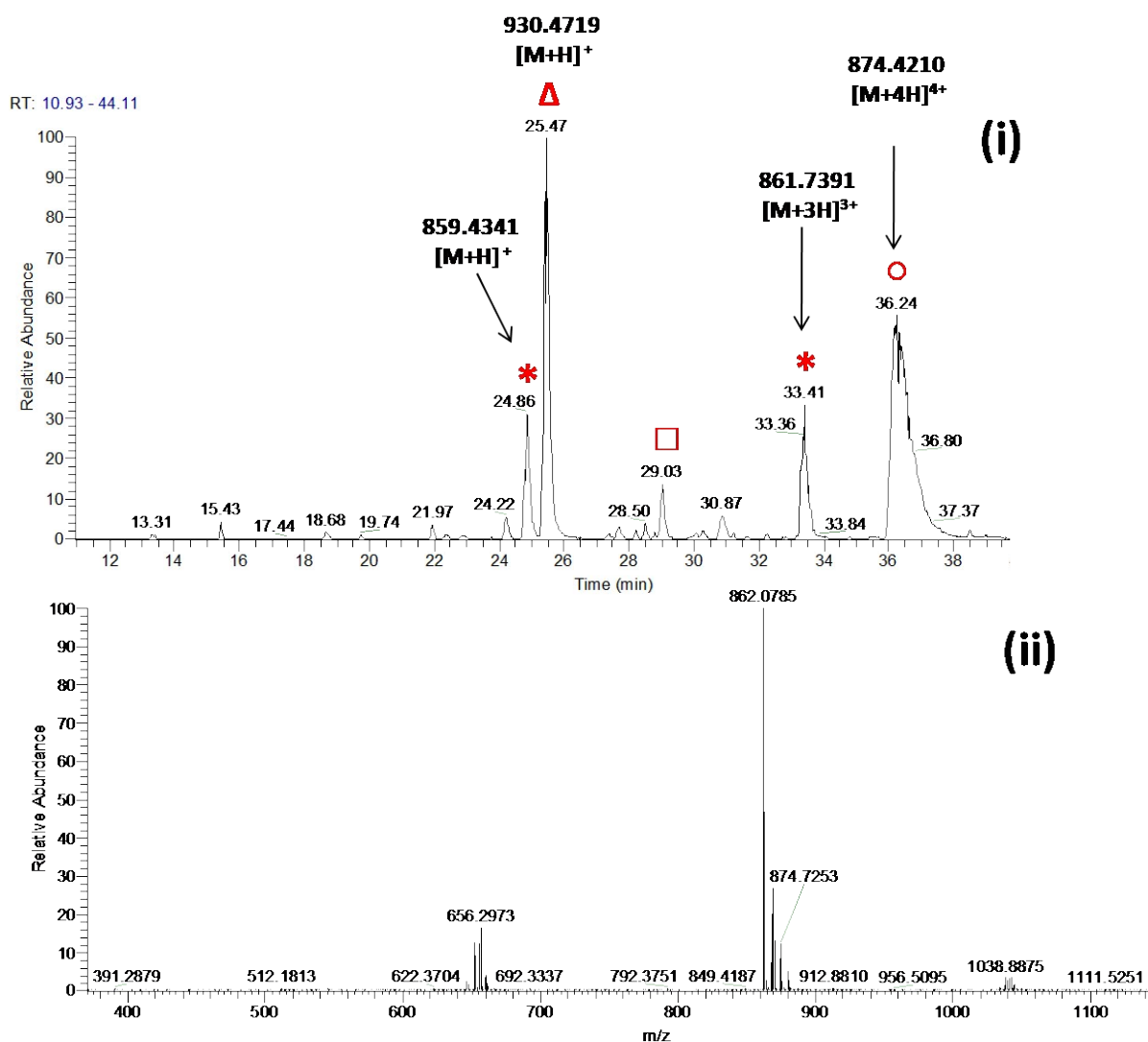


Figure S5: Total base chromatogram for insulin oxidised chain B using an IMER of 150 mm long, using a protein standard concentration of 0.05 mg/mL, and a flow rate of 0.1 μ L/min (i) as well as the corresponding mass spectrum (ii). Peaks are identified as follows: * indicates expected fragments of GFFYTPK, 858.4 Da and FVNQHLC_{ox}GSHLVEALYLVC_{ox}GER, 2583.0 Da, Δ stands for the fragment with uncleaved alanine G²³FFYTPKA³⁰, \square designates the unknown fragment which originates in the standard, and circle denotes the intact protein.

The use of a longer IMER with a reduced standard concentration also resulted in a partial digestion, with a sequence coverage of only 70 %.

References:

1. S. Currivan, D. Connolly and B. Paull, *Microchem J*, 2013, **111**, 32-39.
2. D. S. Peterson, T. Rohr, F. Svec and J. M. J. Fréchet, *J. Proteome. Res.*, 2002, **1**, 563-568.
3. D. S. Peterson, T. Rohr, F. Svec and J. M. J. Fréchet, *Anal. Chem.*, 2002, **74**, 4081-4088.
4. J. Krenkova, Z. Bilková and F. Foret, *J. Sep. Sci.*, 2005, **28**, 1675-1684.

5. M. V. Volokitina, E. G. Vlach, G. A. Platonova, D. O. Vinokhodov and T. B. Tennikova, *J. Sep. Sci.*, 2013, **36**, 2793-2805.
6. C. Yao, L. Qi, W. Hu, F. Wang and G. Yang, *Anal. Chim. Acta*, 2011, **692**, 131-137.
7. J. Spross and A. Sinz, *Anal. Chem.*, 2010, **82**, 1434-1443.
8. M. Naldi, U. Cernigoj, A. Strancar and M. Bartolini, *Talanta*, 2017, **167**, 143-157.
9. J. Ma, Z. Liang, X. Qiao, Q. Deng, D. Tao, L. Zhang and Y. Zhang, *Anal. Chem.*, 2008, **80**, 2949-2956.
10. J. Gao, J. Xu, L. E. Locascio and C. S. Lee, *Anal. Chem.*, 2001, **73**, 2648-2655.
11. J. W. Cooper, J. Chen, Y. Li and C. S. Lee, *Anal. Chem.*, 2003, **75**, 1067-1074.
12. A. Le Nel, J. Krenkova, K. Kleparnik, C. Smadja, M. Taverna, J.-L. Viovy and F. Foret, *Electrophoresis*, 2008, **29**, 4944-4947.
13. E. Bonneil, M. Mercier and K. C. Waldron, *Anal. Chim. Acta*, 2000, **404**, 29-45.
14. C. Wang, R. Oleschuk, F. Ouchen, J. Li, P. Thibault and D. J. Harrison, *Rapid Commun. Mass Spectrom.*, 2000, **14**, 1377-1383.
15. L. Sun, G. Zhu, X. Yan, S. Mou and N. J. Dovichi, *J. Chromatogr. A*, 2014, **1337**, 40-47.
16. A. Kecskemeti and A. Gaspar, *Talanta*, 2017, **166**, 275-283.
17. H. M. Yuan, S. Zhang, B. F. Zhao, Y. J. Weng, X. D. Zhu, S. W. Li, L. H. Zhang and Y. K. Zhang, *Anal. Chem.*, 2017, **89**, 6324-6329.
18. L. Amankwa and W. G. Kuhr, *Anal. Chem.*, 1992, **64**, 1610-1613.
19. E. C. A. Stigter, G. J. De Jong and W. P. Van Bennekom, *Anal. Bioanal. Chem.*, 2007, **389**, 1967-1977.